Machine Learning Approach for Predicting Wall Shear Distribution for Abdominal Aortic Aneurysm and Carotid Bifurcation Models

Milos Jordanski, Milos Radovic, Zarko Milosevic, Nenad Filipovic, and Zoran Obradovic

***Abstract*—Computer simulations based on the finite element method represent powerful tools for modeling blood flow through arteries. However, due to its computational complexity, this approach may be inappropriate when results are needed quickly. In order to reduce computational time, in this paper, we proposed an alternative machine learning based approach for calculation of wall shear stress (WSS) distribution, which may play an important role in mechanisms related to initiation and development of atherosclerosis. In order to capture relationships between geometric parameters, blood density, dynamic viscosity and velocity, and WSS distribution of geometrically parameterized abdominal aortic aneurysm (AAA) and carotid bifurcation models, we proposed multivariate linear regression, multilayer perceptron neural network and Gaussian conditional random fields (GCRF). Results obtained in this paper show that machine learning approaches can successfully predict WSS distribution at different cardiac cycle time points. Even though all proposed methods showed high potential for WSS prediction, GCRF achieved the highest coefficient of determination (0.930–0.948 for AAA model and 0.946–0.954 for carotid bifurcation model) demonstrating benefits of accounting for spatial correlation. The proposed approach can be used as an alternative method for real time calculation of WSS distribution.**

***Index Terms*—Abdominal aortic aneurysm (AAA), carotid bifurcation, finite element (FE) modeling, machine learning, wall shear stress (WSS).**

Manuscript received June 28, 2016; revised October 31, 2016; accepted December 6, 2016. Date of publication; date of current version. This work was supported in part by the Defense Advanced Research Project Agency (DARPA) GRAPHS program through Air Force Research Laboratory (AFRL) under prime Contract FA9550-12-1-0406, in part by the National Science Foundation BIGDATA under Grant 14476570, in part by the Office of Naval Research Mathematics of Data Science Project N00014-15-1-2729, in part by the European Commission SMARTool project 689068, and in part by the Serbian Ministry of Education, Science and Technological Development under Grant III41007 and Grant ON174028. *(M. Jordanski and M. Radovic contributed equally to this work.) (Corresponding author: Z. Obradovic.)*

M. Jordanski is with the Faculty of Mathematics, University of Belgrade, Belgrade 11000, Serbia, and also with the Center for Data Analytics and Biomedical Informatics, College of Science and Technology, Temple University, Philadelphia, PA 19122 USA (e-mail: jordanski90@hotmail.com).

M. Radovic is with the Research and Development Center for Bioengineering BioIRC, Kragujevac 34000, Serbia, and also with the Center for Data Analytics and Biomedical Informatics, College of Science and Technology, Temple University, Philadelphia PA 19122 USA (e-mail: mradovic@kg.ac.rs).

Z. Milosevic is with the Research and Development Center for Bioengineering BioIRC, Kragujevac 34000, Serbia, and also with the Faculty of Engineering, University of Kragujevac, Kragujevac 34000, Serbia (e-mail: zarko@kg.ac.rs).

N. Filipovic is with the Faculty of Engineering, University of Kragujevac, Kragujevac 34000, Serbia (e-mail: fica@kg.ac.rs).

Z. Obradovic is with the Center for Data Analytics and Biomedical Informatics, College of Science and Technology, Temple University, Philadelphia, PA 19122 USA (e-mail: zoran.obradovic@temple.edu).

Digital Object Identifier 10.1109/JBHI.2016.2639818

I. Introduction

STROKE is one of the most common causes of death worldwide. Often it occurs as a result of carotid artery stenosis, which may produce infarction by embolization or thrombosis at the site of narrowing. Local hemodynamics, affecting both thrombosis and embolization processes, can be investigated by computer simulations.

There are many factors that may increase the risk of stroke, such as systolic and diastolic hypertension, cigarette smoking, diabetes, etc. It has been shown that stenosis may occur as a consequence of geometrical vessel dimensions changes in the region of the carotid bifurcation [1], [2]. In fact, these geometrical changes affect blood flow and, thus, the entire local hemodynamics, including wall shear stress (WSS) distribution. Large changes of the WSS values may affect the embolic mechanism by which carotid lesions can induce stroke [3].

An aneurysm is a blood-filled balloon-like bulge in the blood vessel wall usually growing at regions of low WSS [4]. Its rupture can cause severe hemorrhaging and even death. It has been shown that hemodynamics plays a fundamental role in the mechanisms of initiation, growth, and rupture of aneurysm [5].

A number of papers show that WSS has significant impact on atherosclerosis emergence and development processes [6], [7]. Therefore, calculation and analysis of this quantity is of great importance. Simulations based on the finite element (FE) method can accurately calculate WSS distribution. However, this approach may be prohibitively computationally costly in medical applications when results should be provided quickly. For this purpose, alternative approaches based on machine learning algorithms may be more suitable. It has been shown that several machine learning algorithms like neural networks, linear regression, k-nearest neighbors, random forest, and support vector machine have high potential for modeling relationships between WSS and parameters of geometrically parameterized models of abdominal aortic aneurysm (AAA) and carotid bifurcation [8], [9]. However, these algorithms are all unstructured

predictors and do not account for spatial dependencies between output variables (WSS). In addition, previous studies [8], [9] were based on steady state simulation and do not incorporate temporal evolution of WSS.

Unstructured regression is designed to model input–output dependencies disregarding relationships among outputs. Multivariate linear regression (MLR) and multilayer perceptron (MLP) neural network are two techniques commonly used for unstructured regression problems. Unlike MLR, which is a simple model that uses a linear combination of predictor variables to model a continuous response vector, MLP is a complex model in which data from predictor variables flow through a network consisting of multiple layers of nodes called neurons providing the response vector at the output. On the other hand, Gaussian conditional random fields (GCRF) are a type of structured regression model that incorporates multiple predictors and multiple graphs [10]. One of the main problems with structured regression is related to the fact that models are usually not convex and thus, they do not guarantee global optimum and efficient optimization. It has been shown that if the relationships among the outputs are represented in a specific form, then the traditional continuous conditional random field model has the form of a multivariate Gaussian distribution, which facilitates learning and inference. So far, different extensions of GCRF have been developed [11], [12] and GCRF has been successfully applied for solving various challenging problems [13], [14].

In this paper, we evaluated two unstructured prediction models, MLP neural network and MLR, as well as a GCRF model to capture temporal relationships between geometric parameters, blood density, dynamic viscosity and blood velocity (input variables), and WSS distributions (output variable). To analyze the influence of previously mentioned input variables on WSS distributions in the human carotid bifurcation and AAA, computer simulations were run to generate data pertaining to this phenomenon. In this paper, we test the following two hypotheses:

1) WSS distributions at different cardiac cycle time points for geometrically parameterized models of AAA and carotid bifurcation can be modeled by using machine learning approaches.
2) The use of GCRF model for capturing spatial relationships may lead to improvement in overall WSS distributions prediction accuracy when comparing to unstructured predictors.

II. Methodology

A. Datasets

In order to demonstrate the applicability of machine learning techniques for capturing relationships between geometric parameters, density, viscosity and velocity, and WSS distribution, datasets containing 4000 samples for both AAA carotid bifurcation models were created by using in-house software packages [15], [16]. Input variables (predictors) were chosen based on their known influence on WSS calculation. In particular, shear stress in a general laminar flow is proportional to the gradient of fluid velocity in the direction perpendicular to the flow where the dynamic viscosity is a constant of proportionality. In computational fluid dynamics (CFD), governing equations for the blood flow in lumen domain are three-dimensional Navier–Stokes equations (which incorporate the density of the blood and dynamic viscosity) together with the continuity equation [16]. The solution, for a particular set of boundary conditions (e.g., prescribed inlet velocity profile which simulates cardiac cycle), provides the fluid velocity in a given geometry, which is in our case defined by geometric parameters.

TABLE I
AVERAGE VALUES OF INPUT PARAMETERS FOR AAA MODEL

Parameter	Mean value	Unit
Length	100	mm
Aneurysm length	40	mm
A	30	mm
Aorta diameter	20	mm
C	20	mm
B	20	mm
Density	0.00105	gr/mm^3
Dynamic viscosity	0.003675	Pa·s
Peak systolic velocity	300	mm/s

TABLE II
AVERAGE VALUES OF INPUT PARAMETERS FOR CAROTID BIFURCATION MODEL

Parameter	Mean value	Unit
Angle ICA-CCA	25	deg
Angle ECA-CCA	25	deg
Diameter of CCA	6.2	mm
Diameter of CBRE	3.658	mm
Diameter of CBRI	4.9	mm
Length of CCA	7.44	mm
Length of CBR	7.316	mm
Length of ECA	18.6	mm
Length of ICA	26.04	mm
Diameter at end of ICA	4.34	mm
Diameter of ICB	6.49	mm
Distance to ICB	5.39	mm
Density	0.00105	gr/mm^3
Dynamic viscosity	0.00367	Pa·s
Peak systolic velocity	437.22	mm/s

Sampling is performed from uniform distributions with perturbation of each parameter up to 30% of the corresponding mean values [16]. Tables I and II show the mean values of input variables used for sampling of AAA and carotid bifurcation model parameters, respectively.

The geometric parameters shown in Figs. 1 and 2 were used to generate internal blood vessel surfaces. Generated surfaces represent the boundaries for blood flow domain. We assumed that both AAA and carotid bifurcation have the same symmetry plane. Therefore, FE models were generated for half of the domain, but the results can be presented for the entire domain.

Unsteady simulations with parabolic inflow velocity profiles were undertaken and WSS distributions for each geometry were computed for 10 time steps ($N_t = 10$). We assumed the entering flow was pulsatile, with a typical waveforms shown in Fig. 3 for AAA [17] and carotid bifurcation [18] models. For each

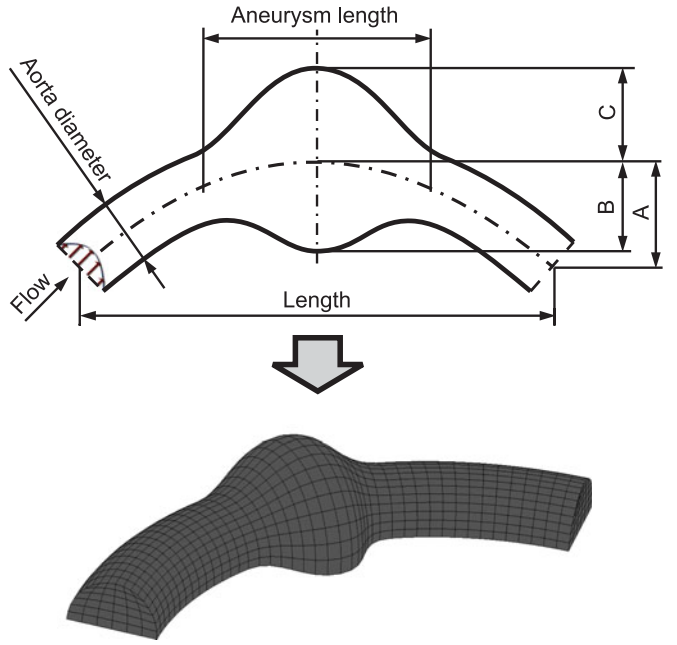

Fig. 1. Geometrically parameterized model of AAA. Geometrical parameters of AAA model: 'Length' is the parameter that defines the total horizontal projection of the generated AAA model; 'A' is the height of the arc of the central line; 'Aorta diameter' is the abdominal aorta diameter; 'B' is the radius from the central line to the inner wall of the aneurysm; 'C' is the radius from the central line to the outer wall of the aneurysm; 'Aneurysm length' is the average length of the aneurysm.

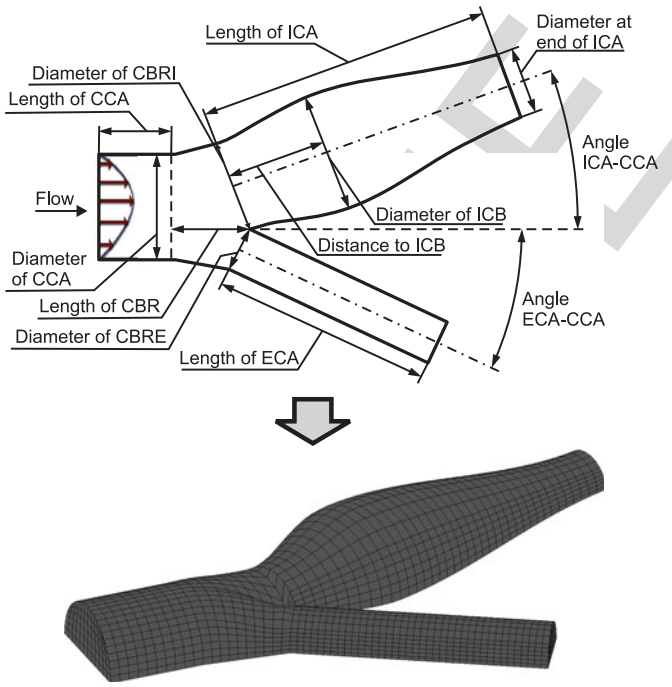

Fig. 2. Geometrically parameterized model of carotid bifurcation. The abbreviations here are: CCA–common carotid artery, CBR–carotid bifurcation region, CBRE–carotid bifurcation region external, ECA–external carotid artery, CBRI–carotid bifurcation region internal, ICA–internal carotid artery, ICB–internal carotid bulbus.

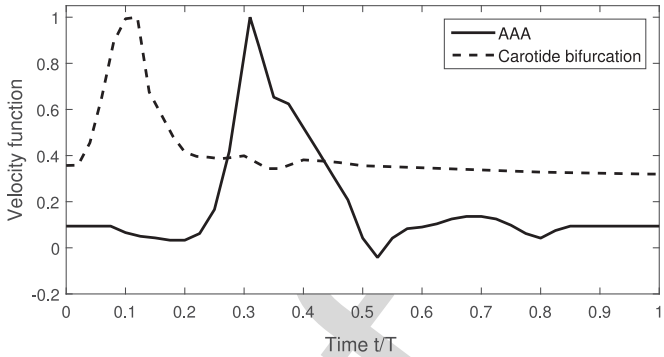

Fig. 3. Input velocity profile for the AAA [17] and carotid bifurcation [18] models. Inlet peak systolic velocity (PSV) corresponds to t/T = 0.305 and t/T = 0.1 for AAA and carotid bifurcation models respectively, where t/T is the relative time with respect to the cycle period T.

generated sample of both aneurysm and carotid bifurcation models, peak systolic velocity is sampled from the uniform distribution (bounded with 30% perturbation of the corresponding mean value) while velocity values in other time steps are calculated by multiplying the sampled peak systolic velocity value with the corresponding function given in Fig. 3. Mean values of the peak systolic velocity for aneurysm and carotid bifurcation models are adopted from [17] and [18], respectively.

All velocity components at the fixed walls are set to be zero. Similarly, the velocity components at the plane of symmetry in the direction normal to the plane, are set to zero. It is assumed that the end cross-sections of both AAA and carotid bifurcation models are stress-free, i.e., normal and tangential stresses are set to zero. The flow was assumed to be laminar, Newtonian, and incompressible. Also, the walls are assumed to be rigid. All calculations were performed using an open source FE program for fluid flow and fluid-solid interaction - PAK [15]. The CFD postprocessing results give an insight into the local hemodynamics and the blood mechanical action on the vessel walls, including the distribution of WSS.

In order to test whether the accuracy of the proposed machine learning based method for prediction of WSS distribution depends on the mesh resolution, we generated three datasets, each containing 4000 samples, with different mesh resolutions for both AAA and carotid bifurcation models. In these datasets, generated samples of the AAA FE model contain 375, 1125, and 2205 nodes, where 195, 597, and 885 lie on the wall surface, respectively. On the other hand, samples of the carotid bifurcation FE model contain 1854, 3877, and 5641 nodes, of which 642, 1303, and 1987 lie on the wall surface respectively. By using CFD simulations, WSS values were calculated in all surface nodes at the vessel wall for all datasets and for all samples for 10 time steps ($N_t = 10$; $t/T = \{0.1, 0.2, \ldots, 1\}$, where t/T is the relative time with respect to the cycle period T).

B. Unstructured Regression

Let us denote by $\mathbf{D} = \{\mathbf{x_i}, \mathbf{y_i}\}_{i=1,\ldots M}$ the dataset containing M observations, where $\mathbf{x_i} = (x_{i1}, \ldots, x_{iP})$ is one

observation with P features and $\mathbf{y_i} = (y_{i1}, \ldots, y_{iN})$ is a vector of real-valued output variables. The aim of multivariate (or multioutput) regression models is to learn a mapping $f : \mathbf{R}^P \rightarrow \mathbf{R}^N$ that predicts the vector of output variables $\mathbf{y_i}$ given an input vector $\mathbf{x_i}$.

1) Multivariate Linear Regression: The MLR model expresses an N-dimensional continuous response vector ($\mathbf{y_i}$) as a linear combination of predictor terms ($\mathbf{x_i}$) plus a vector of error terms ($\epsilon_\mathbf{i}$) with a multivariate normal distribution. In general, model may be written as

$$Y = XW + \epsilon \tag{1}$$

where $\mathbf{Y}$ is a MxN matrix with a series of multivariate measurements, $\mathbf{X}$ is a MxP design matrix, $\mathbf{W}$ is a PxN matrix containing parameters to be estimated, and ϵ is a matrix containing errors or noise. The errors are assumed to be uncorrelated across measurements.

2) MLP Neural Network: The MLP is a prediction model consisting of an input layer, one or more hidden layers and an output layer of simple elements called neurons. Neurons between different layers are connected with parameters called weights, which should be estimated through an optimization procedure (training). The objective of the training is to find a set of neural network parameters that minimize the error between the neural network predictions and the desired outputs. The most commonly used optimization algorithm for learning the parameters of neural network is the back-propagation algorithm [19]. However, the basic version of this algorithm has problems with slow convergence and local minima. For this purpose, a number of variations of the standard algorithm have been developed. In this study, we used the backpropagation algorithm with momentum and adaptive learning rate since it has been shown to be effective for the prediction of the WSS distribution [8], [9]. In each iteration of the this algorithm, parameters of the MLP are adjusted according to the following formula:

$$\Delta W_{\text{new}} = m_c \Delta W_{\text{prev}} + l_r m_c \frac{dE}{dW} \tag{2}$$

where W is a parameter vector, ΔW_{new} and ΔW_{prev} are the new and previous change of the parameter vector, respectively, m_c is a momentum constant, l_r is a learning rate, and E is the objective function which defines how much real outputs disagree with predicted ones (e.g., mean squared error). In each iteration (epoch) of the learning process, the learning rate is adjusted according to l_r^{inc}, l_r^{dec}, and $\max_{\text{inc}}$ parameters. Concretely, if performance decreases toward the goal, the learning rate is increased based on the l_r^{inc} parameter. On the other hand, if performance increases by more than the value defined by the $\max_{\text{inc}}$ parameter, the learning rate is adjusted based on the l_r^{dec} parameter.

In this study, we used an MLP neural network with ten neurons in a single hidden layer and sigmoid activation functions in hidden and output neurons. The stopping criterion was defined as the maximum number of learning epochs (1000). The values of other parameters were: $l_r = 0.01$, $m_c = 0.9$, $l_r^{\text{inc}} = 1.05$, $l_r^{\text{dec}} = 0.7$, and $\max_{\text{inc}} = 1.04$.

C. Structured Regression

A structured learning approach tries to simultaneously predict all outputs given all inputs and relationships among outputs. Structure learning methods can exploit correlation among output variables, which often gives benefits compared to unstructured learning methods. In other words, while traditional, unstructured models use only input information $\mathbf{x}$ to predict y_i, structured learning models use the additional information about y_j, for all j related to i. This prior information about interplays between the outputs $\mathbf{y}$ is application-specific and depends on prior beliefs of a practitioner about which relationships might be useful.

Conditional random fields (CRF) is a type of discriminative probabilistic graphical model designed to predict structured output. Originally, CRF were proposed for classification of sequential data [20].

The conditional distribution $P(\mathbf{y}|\mathbf{x})$ for CRF can be represented as

$$P(\mathbf{y}|\mathbf{x}) = \frac{1}{Z(\alpha, \beta, \mathbf{x})} e^{\sum_{i=1}^{N} A(\alpha, y_i, \mathbf{x}) + \sum_{i \sim j} I(\beta, y_i, y_j, \mathbf{x})} \tag{3}$$

where $A(\alpha, y_i, \mathbf{x})$ is an association potential with parameters α, $I(\beta, y_i, y_j, \mathbf{x})$ is an interaction potential with parameters β, $i \sim j$ denotes that y_i and y_j are connected by an edge in the graph structure, and $Z(\alpha, \beta, \mathbf{x})$ represents a normalization function. In general, the output y_i is associated with a vector of observation $\mathbf{x}$ by an association function, while relationships among outputs can be modeled by an interaction function. Association and interaction potential are usually defined as linear combinations of a set of feature functions over *K*-dimensional parameters α and *L*-dimensional parameters β [20]:

$$A(\alpha, y_i, \mathbf{x}) = \sum_{k=1}^{K} \alpha_k f_k(y_i, \mathbf{x}) \tag{4}$$

$$I(\beta, y_i, y_j, \mathbf{x}) = \sum_{l=1}^{L} \beta_l g_l(y_i, y_j, \mathbf{x}). \tag{5}$$

Feature functions are convenient since they allow one to model arbitrary interplays between inputs and outputs. In this way, any potentially relevant feature may be included to the model since their relevance is automatically determined through the parameter estimation process.

The learning task is to determine values of parameters α and β to maximize the conditional log-likelihood of the set of training examples:

$$L(\alpha, \beta) = \log P(\mathbf{y}|\mathbf{x}) \tag{6}$$

$$(\hat{\alpha}, \hat{\beta}) = \text{argmax}_{\alpha,\beta}(L(\alpha, \beta)). \tag{7}$$

On the other hand, given estimated parameters $\hat{\alpha}$ and $\hat{\beta}$ and inputs $\mathbf{x}$, the inference task is to find the point estimate $\hat{\mathbf{y}}$ of outputs $\mathbf{y}$ such that the conditional probability $P(\mathbf{y}|\mathbf{x})$ is maximized:

$$\hat{\mathbf{y}} = \text{argmax}_{\mathbf{y}}(P(\mathbf{y}|\mathbf{x})). \tag{8}$$

Models with real valued outputs pose quite different challenges with respect to feature function complexity compared to discrete-valued case. CRFs were originally designed for classification problems where the normalizing function Z is finite and defined as a sum over finitely many possible values of $\mathbf{y}$. On the contrary, for regression, Z must be an integrable function. In general, providing that Z is integrable can be very difficult and computationally expensive due to the complexity of association and interaction potentials. However, the association and interaction potentials could be designed in a way that allows efficient learning and inference.

The selection of appropriate feature functions in CRF is a manual process which is usually application-specific. However, the choice of features is often constrained to simple constructs to reduce the complexity of learning and inference from CRF. Let us assume we are given K *unstructured (baseline) predictors*, $R_k(\mathbf{x})$, k $= 1$, ...K, that predict single output y_i relying on any subset of $\mathbf{x}$. To model the dependency between the prediction and output, we use quadratic feature functions:

$$f_k(y_i, \mathbf{x}) = -(y_i - R_k(\mathbf{x}))^2. \tag{9}$$

These feature functions follow the basic principle for association potentials, i.e., their values are large when predictions and outputs are similar. To model the correlation among outputs, we use the quadratic feature function:

$$g_l(y_i, y_j, \mathbf{x}) = -e^l_{\mathrm{ij}} S^l_{\mathrm{ij}}(\mathbf{x})(y_i - y_j)^2 \tag{10}$$

where $e_{ij} = 1$ if an edge exists between output y_i and y_j in the graph G_l, and $e_{ij} = 0$ otherwise; $S^l_{ij}(\mathbf{x})$ represents the similarity between outputs y_i and y_j and in general depends on inputs $\mathbf{x}$. The larger the value of $S^l_{ij}(\mathbf{x})$ is, the more similar the outputs y_i and y_j are. It should be noted that using multiple graphs G_l can facilitate modeling of different aspects of correlation between outputs.

In this way, the exponent of the probability distribution $P(\mathbf{y}|\mathbf{x})$ is a quadratic function in terms of $\mathbf{y}$. Therefore $P(\mathbf{y}|\mathbf{x})$ can be transformed into the multivariate Gaussian distribution $\mathcal{N}(\mu(\mathbf{x}), \mathbf{\Sigma}(\mathbf{x}))$:

$$P(\mathbf{y}|\mathbf{x}) = \frac{1}{(2\pi)^{N/2}\,|\mathbf{\Sigma}|^{1/2}} \times \exp\left(-\frac{1}{2}(\mathbf{y}-\mu)^T \mathbf{\Sigma}^{-1}(\mathbf{y}-\mu)\right) \tag{11}$$

where $\mathbf{\Sigma}$ and μ are covariance matrix and mean vector, respectively. Therefore, the resulting conditional distribution is Gaussian with mean μ and covariance $\mathbf{\Sigma}$. We observe that $\mathbf{\Sigma}$ is a function of parameters α and β, and interaction potential graphs G_l, while μ is also a function of inputs $\mathbf{x}$. The resulting CRF is the Gaussian CRF.

Since the model is Gaussian, the inference is straightforward, i.e., the prediction is expected value, which is equal to the mean μ of the distribution:

$$\hat{\mathbf{y}} = \mathrm{argmax}_{\mathbf{y}} P(\mathbf{y}|\mathbf{x}) = \mathbf{\Sigma}\mathbf{b}. \tag{12}$$

III. Results

A. Evaluation Procedure

In this paper, we employed two unstructured models, MLP neural network and the MLR model, as well as GCRF, in order to predict WSS distributions through time. For training the GCRF model, we randomly chose 70% of total data and remaining 30% of data was used for testing. Since we use predictions of both unstructured models MLP and MLR as inputs to GCRF, we applied fivefold cross validation on the training set. First, for both AAA and carotid bifurcation, we split the training set into five subsets $(D_i, i = 1, \ldots, 5)$ of equal sizes. Then, we reserved one dataset D_i for testing and merged data from the remaining four datasets $D_j, j \neq i$ for training. The procedure was repeated five times, for $i = 1, \ldots, 5$. Finally, we got MLP and MLR predictions for all samples in training sets.

For each surface node, we constructed one MLR model with N_t outputs, where each of N_t outputs represent WSS value for a single time step (N_t is the number of time steps). This means that we created 195, 597, and 885 (642, 1303, and 1987) different linear models in case of the AAA (carotid bifurcation) model. The features of the MLR model were geometric parameters of models, blood density, dynamic viscosity and velocities in all time steps. More specifically, we used 18 features in of the AAA model and 24 features in case of the carotid bifurcation model. The same procedure is repeated for the MLP model where we create one neural network for each node.

In order to employ the GCRF model to predict WSS distribution, we define the similarity matrix (graph) between different surface nodes. Let $S_i = (x_i, y_i, z_i)$ and $S_j = (x_j, y_j, z_j)$ be coordinates of the ith and jth surface nodes, respectively. The distance between two nodes is calculated as the Euclidean distance:

$$d(S_i, S_j) = \sqrt{(x_i - x_j)^2 + (y_i - y_j)^2 + (z_i - z_j)^2}. \tag{13}$$

In order to eliminate noise in the similarity matrix, we eliminated similarities of some nodes that are far away from each other. We calculate similarity matrix between the ith and jth node as

$$S(i,j) = \begin{cases} 0, & \text{if } d(S_i, S_j) > \mu_d \\ 1 - \dfrac{d(S_i, S_j) - \min_d}{\mu_d - \min_d}, & \text{otherwise} \end{cases} \tag{14}$$

where $\min_d$, and μ_d are minimum and mean values of all distances between nodes, respectively.

For each training example and for each time step, we trained a different GCRF model. In this way, we estimated different parameters α and β for each training example. Our proposed model predicts the target values for a test example in the following way. First, it finds the most similar training example (the nearest neighbor) and then uses its estimated parameters α and β to predict the evolution of WSS distributions through time.

We evaluated the performances of the proposed models by computing their coefficients of determination R^2. In a general form, R^2 can be seen as the fraction of unexplained variance. In order to define the coefficient of determination at tth time step

TABLE III
PERFORMANCES FOR AAA MODEL

Dataset (nodes)	Model	t_1	t_2	t_3	t_4	t_5	t_6	t_7	t_8	t_9	t_{10}	Average
AAA (375)	MLR	0.964	0.963	0.957	0.936	0.857	0.765	0.850	0.745	0.827	0.837	0.870
	MLP	0.948	0.982	0.982	0.971	0.934	**0.898**	0.931	**0.883**	0.887	0.806	0.922
	GCRF	**0.969**	**0.984**	**0.984**	**0.972**	**0.935**	**0.898**	**0.932**	**0.883**	**0.894**	**0.853**	**0.930**
AAA (1125)	MLR	0.957	0.960	0.957	0.939	0.939	0.774	0.868	0.734	0.849	0.855	0.883
	MLP	**0.988**	**0.987**	0.990	0.985	0.985	0.862	0.953	0.766	0.917	0.865	0.930
	GCRF	0.986	**0.987**	**0.991**	**0.987**	**0.987**	**0.875**	**0.955**	**0.814**	**0.922**	**0.894**	**0.940**
AAA (2205)	MLR	0.955	0.956	0.953	0.933	0.851	0.774	0.861	0.739	0.842	0.839	0.870
	MLP	0.961	0.982	0.986	0.976	0.940	**0.929**	0.965	0.883	0.944	0.858	0.942
	GCRF	**0.974**	**0.983**	**0.988**	**0.978**	**0.942**	**0.929**	**0.966**	**0.885**	**0.945**	**0.886**	**0.948**

TABLE IV
PERFORMANCES FOR CAROTID BIFURCATION MODEL

Dataset (nodes)	Model	t_1	t_2	t_3	t_4	t_5	t_6	t_7	t_8	t_9	t_{10}	Average
Carotid (1854)	MLR	0.767	0.740	0.761	0.762	0.762	0.763	0.762	0.763	0.763	0.764	0.761
	MLP	0.873	0.930	**0.963**	**0.968**	**0.980**	**0.978**	0.957	0.946	0.932	0.879	0.941
	GCRF	**0.904**	**0.934**	0.960	**0.968**	**0.980**	**0.978**	**0.959**	**0.950**	**0.937**	**0.909**	**0.948**
Carotid (3877)	MLR	0.803	0.768	0.768	0.768	0.793	0.794	0.794	0.794	0.795	0.795	0.787
	MLP	0.850	0.891	**0.966**	**0.985**	**0.985**	**0.985**	**0.982**	**0.964**	0.911	0.880	0.940
	GCRF	**0.908**	**0.914**	**0.966**	**0.985**	**0.985**	**0.985**	0.979	**0.964**	**0.933**	**0.917**	**0.954**
Carotid (5641)	MLR	0.791	0.762	0.781	0.782	0.782	0.782	0.782	0.782	0.783	0.783	0.781
	MLP	0.845	**0.910**	0.960	**0.980**	**0.983**	**0.974**	**0.974**	**0.959**	**0.945**	0.831	0.936
	GCRF	**0.895**	**0.910**	**0.961**	0.973	**0.983**	**0.974**	**0.974**	**0.959**	**0.945**	**0.891**	**0.946**

R_t^2, let us define $\overline{y}^t(j)$ as the mean value of WSS for the jth surface node at time step t:

$$\overline{y}^t(j) = \frac{1}{N_{\text{test}}} \sum_{i=1}^{N_{\text{test}}} y_i^t(j),$$
$$t = 1, \ldots N_t, j = 1, \ldots, N_{\text{surf}} \quad (15)$$

where N_{test} is the number of testing examples, N_{surf} is the number of surface nodes, and $y_i^t(j)$ is the WSS value for jth node at tth time step of ith example calculated by the finite element method (FEM). The sum of squares (proportional to the variances) $\overline{SE}_i^t$ for the ith example at time step t is calculated as

$$\overline{SE}_i^t = \sum_{j=1}^{N_{\text{surf}}} (y_i^t(j) - \overline{y}^t(j))^2. \quad (16)$$

The residuals are defined as a squared error of the ith example at time step t:

$$SE_i^t = \sum_{j=1}^{N_{\text{surf}}} (y_i^t(j) - \hat{y}_i^t(j))^2 \quad (17)$$

where $\hat{y}_i^t(j)$ is the predicted WSS value for jth surface node at tth time step of ith example. Finally, the coefficient of determination R_t^2 at tth time step is calculated as

$$R_t^2 = 1 - \frac{\sum_{i=1}^{N_{\text{test}}} SE_i^t}{\sum_{i=1}^{N_{\text{test}}} \overline{SE}_i^t}. \quad (18)$$

B. Performance on AAA and Carotid Bifurcation

In order to make a fair comparison, we trained unstructured models (MLP neural network and MLR) on the same data used for GCRF training. Tables III and IV show obtained results on the same test data for AAA and carotid bifurcation models, respectively. Values in these tables represent coefficient of determination R_t^2, for each time step $t = 1, \ldots, 10$, along with the average R^2 across all time steps.

Tables III and IV clearly show that the MLP model outperforms the MLR model on both AAA and carotid bifurcation models. More precisely, on the AAA(375) dataset, the MLP achieved higher accuracy compared to the MLR in eight out of ten time steps. In addition, on the AAA(1125) and AAA(2205) datasets, the MLP outperformed the MLR in all time steps. Similar results are obtained on carotid bifurcation datasets where the MLP achieved higher accuracy compared to the MLR in all time steps for all three mesh resolutions (1854, 3877, and 5641 nodes). The fact that the MLP improved accuracy over the MLR model is confirmed by the average R^2 values across all time steps (the last columns in Tables III and IV). Even though the MLP outperforms the MLR on all datasets, results given in Tables III and IV indicate that both the MLP (better) and the MLR (worse) can be used to predict WSS distribution through time. This confirms the first hypothesis of our paper that WSS distributions at different cardiac cycle time points for geometrically parameterized models of AAA and carotid bifurcation can be modeled by using machine learning approaches.

In addition, Tables III and IV show that the GCRF model achieved higher accuracy compared to unstructured predictors

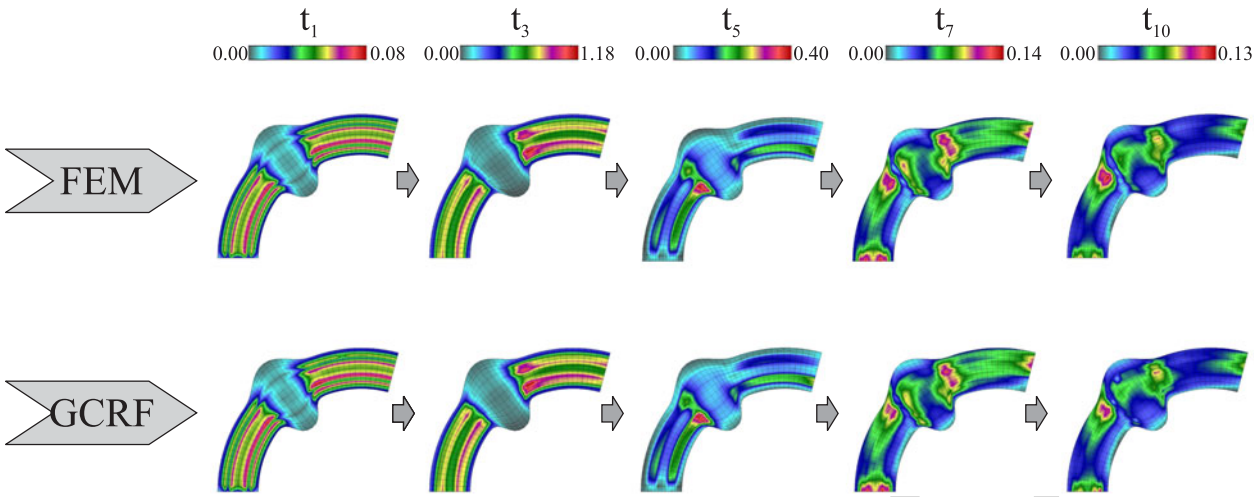

Fig. 4. Temporal evolution of WSS distribution for the AAA model (one randomly chosen geometry) calculated by FEM and predicted by the GCRF (units Pa). Due to space limitation we show results for only five time steps (of total ten).

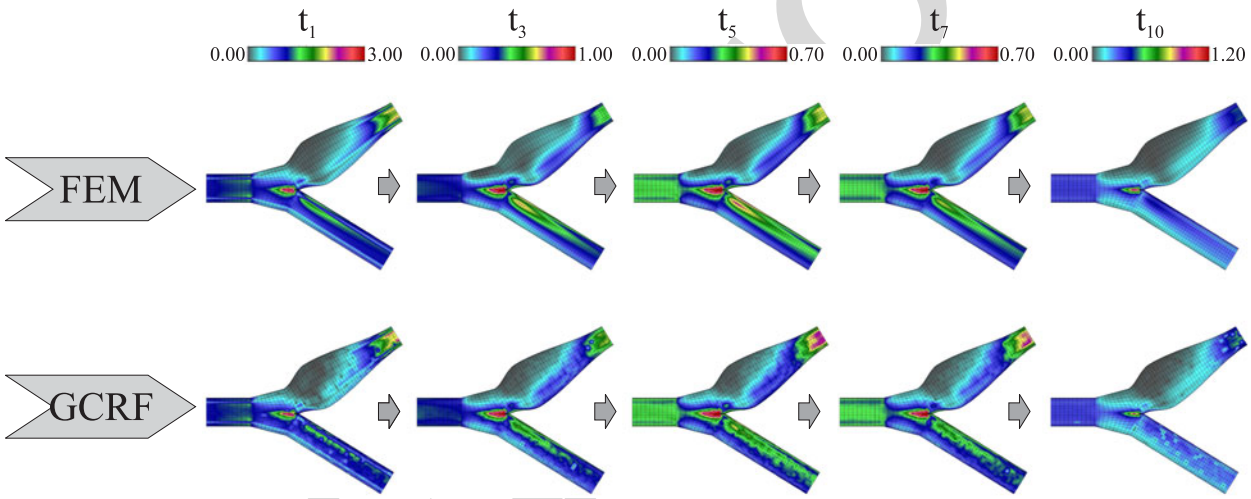

Fig. 5. Temporal evolution of WSS distribution for the carotid bifurcation model (one randomly chosen geometry) calculated by FEM and predicted by the GCRF (units Pa). Due to space limitation we show results for only five time steps (of total ten).

(MLP and MLR) on both datasets. More precisely, on the AAA(375) dataset, the GCRF outperformed the MLP model in eight out of ten time steps, while on the remaining two steps they achieved the same accuracy. Furthermore, on AAA(1124) dataset, the GCRF achieved higher accuracy compared to the MLP model in eight out of ten time steps, while on one step they achieved the same accuracy. Similarly, on the AAA(2205) dataset, the GCRF achieved higher accuracy compared to the MLP model in nine out of ten time steps, while on the remaining step they achieved the same accuracy. Similar results can be observed on the carotid bifurcation dataset. More specifically, on Carotid(1854) dataset, the GCRF outperformed the MLP model in six out of ten time steps, while they achieved the same accuracy in three steps. Similarly, on the Carotid(3877) dataset, the GCRF achieved higher accuracy compared to the MLP model in four out of ten time steps, while they achieved the same accuracy in five time steps. On the Carotid(5641) dataset, GCRF outperformed the MLP model in three out of ten time steps, while they achieved the same accuracy six steps. In addition, GCRF outperformed MLR in all time steps for all AAA and carotid bifurcation datasets. The average values of R^2 calculated across all time steps show that the GCRF model outperformed both unstructured predictors. These results confirm the second hypothesis of our paper, i.e., taking spatial correlation into account improves prediction accuracy of WSS distribution through time.

Figs. 4 and 5 show the distribution of WSS through time, calculated by FEM and predicted by the GCRF model. Due to lack of space, we showed results only for one randomly chosen test example from AAA and carotid bifurcation datasets in five time steps (t_1, t_3, t_5, t_7, and t_{10}). These figures confirm the ability of machine learning approaches to predict the WSS distribution through time for both geometrically parameterized models.

In addition, we compared running time of FEM and GCRF methods for prediction of WSS distribution of AAA and carotid

bifurcation models. Training of the GCRF model for prediction of WSS distribution is a tedious task. However, once trained this model can be utilized to predict WSS distribution in much shorter time when comparing to FEM approach. For instance, average FEM run time for calculation of WSS distribution of testing samples was 5.3, 6.8, and 8.0 s for the three datasets of the AAA model and 19.4, 198.4, and 604.1 for the three datasets of the carotid bifurcation model. On the other hand, the corresponding average GCRF run times were 0.032, 0.283, and 0.604 s for the AAA model and 0.5702, 5.856, and 10.937 for the carotid bifurcation model. All the experiments were run on a Windows machine with a 3.40 GHz Intel(R) Core(TM) i7-3770 CPU and 32GB memory.

IV. Conclusion

In this paper, an application of machine learning techniques to hemodynamic problems was presented. We modeled the relationships between geometric parameters, blood density, dynamic viscosity and velocity of the human carotid bifurcation, and AAA models and the WSS distribution. The goal of this paper is to verify that for geometrically parameterized models, which are simplified comparing to real geometries, machine learning approaches may be used to predict WSS distribution at different cardiac cycle time points. We employed two unstructured predictors, MLP neural network and the MLR model, in order to predict WSS distributions through time. The obtained results showed that on the AAA model both predictors exhibited capabilities of being used for this task, while on the carotid bifurcation model MLP demonstrated much better results in terms of R^2. In addition, we applied the GCRF model, which leverages the benefits of both unstructured models as well as the similarities between different surface nodes. The results obtained from simulations showed that GCRF was able to improve accuracy on both AAA and carotid bifurcation models. Furthermore, this work shows that the achieved results can be used to aid the assessment of stroke risk for a given patient's data in real time.

Further research will be focused on applying other unstructured multioutput regression models and including them into the GCRF model. In addition, since we used simplified geometrically parameterized models, our further research plan is to use real life data, where machine learning techniques will be tested on patient data. More specifically, we plan to represent a real arterial geometry with an adequate geometrically parameterized model and predict WSS distribution for the simplified model. Thereafter, WSS value of each surface node of the real arterial geometry can be estimated by interpolating WSS values of the nearest nodes of the simplified model. However, real arterial geometries are quite complex and describing them with a set of features that can be further processed by machine learning methods to predict WSS distribution is a challenging task. Therefore, we plan to extend the proposed approach where, in addition to geometrical parameters which can be estimated from medical images, machine learning approaches would also use other node specific descriptors (e.g., coordinates, distance from the central line, local curvature descriptors, cross section area, etc.) to predict the WSS value. In this case, instead of node specific predictors, we would generate a global predictor which would predict WSS values for all nodes belonging to a certain arterial region (for instance all nodes in the internal carotid bulbus region).

References

[1] U. G. Schulz and P. M. Rothwell, "Sex differences in carotid bifurcation anatomy and the distribution of atherosclerotic plaque," *Stroke*, vol. 32, no. 47, pp. 1525–1531, Jul. 2001.

[2] U. G. Schulz and P. M. Rothwell, "Major variation in carotid bifurcation anatomy: a possible risk factor for plaque development," *Stroke*, vol. 32, no. 11, pp. 2522–2529, Nov. 2001.

[3] S. Lorthois, P. Lagree, J. Marc-Vergnes, and F. Cassot, "Maximal wall shear stress in arterial stenoses: Application to the internal carotid arteries," *ASME J. Biomech. Eng.*, vol. 12, pp. 661–666, 2000.

[4] L. Boussel *et al.*, "Aneurysm growth occurs at region of low wall shear stress: Patientspecific correlation of hemodynamics and growth in a longitudinal study," *Stroke*, vol. 38, no. 11, pp. 2997–3002, 2008.

[5] J. Xiang *et al.*, "Hemodynamic-morphologic discriminants for intracranial aneurysm rupture," *Stroke*, vol. 42, no. 1, pp. 144–152, 2011.

[6] A. Malek, S. Alper, and S. Izumo, "Hemodynamic shear stress and its role in atherosclerosis," *J. Amer. Med. Assoc.*, vol. 282, no. 21, pp. 2035–2042, 1999.

[7] M. Akram and J. Andre, "Wall shear stress and early atherosclerosis," *Amer. J. Roentgenology*, vol. 174, no. 6, pp. 1657–1665, 2000.

[8] M. Radovic, D. Petrovic, and N. Filipovic, "Mining data from cfd simulation for aneurysm and carotid bifurcation models," in *Proc. 33rd Annu. Int. Conf. IEEE Eng. Med. Biol. Soc.*, Sep. 2011, pp. 8311–8314.

[9] Z. Bosnic, P. Vracar, M. Radovic, G. Devedzic, N. Filipovic, and I. Kononenko, "Mining data from hemodynamic simulations for generating prediction and explanation models," *IEEE Trans. Inf. Technol. Biomed.*, vol. 16, no. 2, pp. 248–254, Mar. 2012.

[10] V. Radosavljevic, S. Vucetic, and Z. Obradovic, "Continuous conditional random fields for regression in remote sensing," in *Proc. 2010 19th Eur. Conf. Artif. Intell.*, 2010, pp. 809–814.

[11] J. Glass, M. Ghalwash, M. Vukicevic, and Z. Obradovic, "Extending the modeling capacity of gaussian conditional random fields while learning faster," in *Proc. 30th AAAI Conf. Artif. Intell.*, Feb. 2016, pp. 1–4.

[12] J. Slivka, M. Nikolic, K. Ristovski, V. Radosavljevic, and Z. Obradovic, "Distributed gaussian conditional random fields based regression for large evolving graphs," in *Proc. 14th SIAM Int. Conf. Data Mining, Workshop Mining Netw. Graphs*, Apr. 2014.

[13] N. Djuric, V. Radosavljevic, Z. Obradovic, and S. Vucetic, "Gaussian conditional random fields for aggregation of operational aerosol retrievals," *IEEE Geosci. Remote Sens. Lett.*, vol. 12, no. 4, pp. 761–765, Apr. 2015.

[14] A. Polychronopoulou and Z. Obradovic, "Hospital pricing estimation by gaussian conditional random fields based regression on graphs," in *Proc. 2014 IEEE Int. Conf. Bioinformat. Biomed.*, Nov. 2014, pp. 564–567.

[15] M. Kojic, N. Filipovic, R. Slavkovic, M. Zivkovic, and N. Grujovic, "Pak-fs - Finite element program for fluid flow and fluid-solid interaction," University of Kragujevac and R&D Center for Bioengineering, Kragujevac, Serbia, 1998.

[16] M. Kojic, N. Filipovic, B. Stojanovic, and N. Kojic, *Computer Modeling in Bioengineering: Theoretical Background, Examples and Software*. Hoboken, NJ, USA: Wiley, 2008.

[17] C. M. Scotti, A. D. Shkolnik, S. C. Muluk, and E. A. Finol, "Fluid-structure interaction in abdominal aortic aneurysms: effects of asymmetry and wall thickness," *Biomed. Eng. Online*, vol. 4, 2005, Art. no. 64.

[18] K. Perktold, M. Resch, and R. O. Peter, "Three-dimensional numerical analysis of pulsatile flow and wall shear stress in the carotid artery bifurcation," *J. Biomech.*, vol. 24, no. 6, pp. 409–420, 1991.

[19] D. E. Rumelhart, G. E. Hinton, and R. J. Williams, *Parallel Distributed Processing: Explorations in the Microstructure of Cognition*, vol. 1, D. E. Rumelhart, J. L. McClelland, and C. PDP Research Group, Eds. Cambridge, MA, USA: MIT Press, 1986.

[20] J. D. Lafferty, A. McCallum, and F. C. N. Pereira, "Conditional random fields: Probabilistic models for segmenting and labeling sequence data," in *Proc. 18th Int. Conf. Mach. Learn.*, 2001, pp. 282–289.

Authors' photographs and biographies not available at the time of publication.

Queries

Q1. Authors: When accessing and uploading your corrections at the Author Gateway, please note we cannot accept new source files as corrections for your paper. Please do not send new Latex, Word, or PDF files, as we cannot simply "overwrite" your paper. Please submit your corrections as an annotated PDF or as clearly written list of corrections, with location in paper. You can also upload revised graphics to the Gateway.

Q2. Author: Please provide page range in Ref. [12].

Machine Learning Approach for Predicting Wall Shear Distribution for Abdominal Aortic Aneurysm and Carotid Bifurcation Models

Milos Jordanski, Milos Radovic, Zarko Milosevic, Nenad Filipovic, and Zoran Obradovic

***Abstract*—Computer simulations based on the finite element method represent powerful tools for modeling blood flow through arteries. However, due to its computational complexity, this approach may be inappropriate when results are needed quickly. In order to reduce computational time, in this paper, we proposed an alternative machine learning based approach for calculation of wall shear stress (WSS) distribution, which may play an important role in mechanisms related to initiation and development of atherosclerosis. In order to capture relationships between geometric parameters, blood density, dynamic viscosity and velocity, and WSS distribution of geometrically parameterized abdominal aortic aneurysm (AAA) and carotid bifurcation models, we proposed multivariate linear regression, multilayer perceptron neural network and Gaussian conditional random fields (GCRF). Results obtained in this paper show that machine learning approaches can successfully predict WSS distribution at different cardiac cycle time points. Even though all proposed methods showed high potential for WSS prediction, GCRF achieved the highest coefficient of determination (0.930–0.948 for AAA model and 0.946–0.954 for carotid bifurcation model) demonstrating benefits of accounting for spatial correlation. The proposed approach can be used as an alternative method for real time calculation of WSS distribution.**

***Index Terms*—Abdominal aortic aneurysm (AAA), carotid bifurcation, finite element (FE) modeling, machine learning, wall shear stress (WSS).**

Manuscript received June 28, 2016; revised October 31, 2016; accepted December 6, 2016. Date of publication; date of current version. This work was supported in part by the Defense Advanced Research Project Agency (DARPA) GRAPHS program through Air Force Research Laboratory (AFRL) under prime Contract FA9550-12-1-0406, in part by the National Science Foundation BIGDATA under Grant 14476570, in part by the Office of Naval Research Mathematics of Data Science Project N00014-15-1-2729, in part by the European Commission SMARTool project 689068, and in part by the Serbian Ministry of Education, Science and Technological Development under Grant III41007 and Grant ON174028. *(M. Jordanski and M. Radovic contributed equally to this work.) (Corresponding author: Z. Obradovic.)*

M. Jordanski is with the Faculty of Mathematics, University of Belgrade, Belgrade 11000, Serbia, and also with the Center for Data Analytics and Biomedical Informatics, College of Science and Technology, Temple University, Philadelphia, PA 19122 USA (e-mail: jordanski90@hotmail.com).

M. Radovic is with the Research and Development Center for Bioengineering BioIRC, Kragujevac 34000, Serbia, and also with the Center for Data Analytics and Biomedical Informatics, College of Science and Technology, Temple University, Philadelphia PA 19122 USA (e-mail: mradovic@kg.ac.rs).

Z. Milosevic is with the Research and Development Center for Bioengineering BioIRC, Kragujevac 34000, Serbia, and also with the Faculty of Engineering, University of Kragujevac, Kragujevac 34000, Serbia (e-mail: zarko@kg.ac.rs).

N. Filipovic is with the Faculty of Engineering, University of Kragujevac, Kragujevac 34000, Serbia (e-mail: fica@kg.ac.rs).

Z. Obradovic is with the Center for Data Analytics and Biomedical Informatics, College of Science and Technology, Temple University, Philadelphia, PA 19122 USA (e-mail: zoran.obradovic@temple.edu).

Digital Object Identifier 10.1109/JBHI.2016.2639818

I. Introduction

STROKE is one of the most common causes of death worldwide. Often it occurs as a result of carotid artery stenosis, which may produce infarction by embolization or thrombosis at the site of narrowing. Local hemodynamics, affecting both thrombosis and embolization processes, can be investigated by computer simulations.

There are many factors that may increase the risk of stroke, such as systolic and diastolic hypertension, cigarette smoking, diabetes, etc. It has been shown that stenosis may occur as a consequence of geometrical vessel dimensions changes in the region of the carotid bifurcation [1], [2]. In fact, these geometrical changes affect blood flow and, thus, the entire local hemodynamics, including wall shear stress (WSS) distribution. Large changes of the WSS values may affect the embolic mechanism by which carotid lesions can induce stroke [3].

An aneurysm is a blood-filled balloon-like bulge in the blood vessel wall usually growing at regions of low WSS [4]. Its rupture can cause severe hemorrhaging and even death. It has been shown that hemodynamics plays a fundamental role in the mechanisms of initiation, growth, and rupture of aneurysm [5].

A number of papers show that WSS has significant impact on atherosclerosis emergence and development processes [6], [7]. Therefore, calculation and analysis of this quantity is of great importance. Simulations based on the finite element (FE) method can accurately calculate WSS distribution. However, this approach may be prohibitively computationally costly in medical applications when results should be provided quickly. For this purpose, alternative approaches based on machine learning algorithms may be more suitable. It has been shown that several machine learning algorithms like neural networks, linear regression, k-nearest neighbors, random forest, and support vector machine have high potential for modeling relationships between WSS and parameters of geometrically parameterized models of abdominal aortic aneurysm (AAA) and carotid bifurcation [8], [9]. However, these algorithms are all unstructured

predictors and do not account for spatial dependencies between output variables (WSS). In addition, previous studies [8], [9] were based on steady state simulation and do not incorporate temporal evolution of WSS.

Unstructured regression is designed to model input–output dependencies disregarding relationships among outputs. Multivariate linear regression (MLR) and multilayer perceptron (MLP) neural network are two techniques commonly used for unstructured regression problems. Unlike MLR, which is a simple model that uses a linear combination of predictor variables to model a continuous response vector, MLP is a complex model in which data from predictor variables flow through a network consisting of multiple layers of nodes called neurons providing the response vector at the output. On the other hand, Gaussian conditional random fields (GCRF) are a type of structured regression model that incorporates multiple predictors and multiple graphs [10]. One of the main problems with structured regression is related to the fact that models are usually not convex and thus, they do not guarantee global optimum and efficient optimization. It has been shown that if the relationships among the outputs are represented in a specific form, then the traditional continuous conditional random field model has the form of a multivariate Gaussian distribution, which facilitates learning and inference. So far, different extensions of GCRF have been developed [11], [12] and GCRF has been successfully applied for solving various challenging problems [13], [14].

In this paper, we evaluated two unstructured prediction models, MLP neural network and MLR, as well as a GCRF model to capture temporal relationships between geometric parameters, blood density, dynamic viscosity and blood velocity (input variables), and WSS distributions (output variable). To analyze the influence of previously mentioned input variables on WSS distributions in the human carotid bifurcation and AAA, computer simulations were run to generate data pertaining to this phenomenon. In this paper, we test the following two hypotheses:

1) WSS distributions at different cardiac cycle time points for geometrically parameterized models of AAA and carotid bifurcation can be modeled by using machine learning approaches.
2) The use of GCRF model for capturing spatial relationships may lead to improvement in overall WSS distributions prediction accuracy when comparing to unstructured predictors.

II. Methodology

A. Datasets

In order to demonstrate the applicability of machine learning techniques for capturing relationships between geometric parameters, density, viscosity and velocity, and WSS distribution, datasets containing 4000 samples for both AAA carotid bifurcation models were created by using in-house software packages [15], [16]. Input variables (predictors) were chosen based on their known influence on WSS calculation. In particular, shear stress in a general laminar flow is proportional to the gradient of fluid velocity in the direction perpendicular to the flow where the dynamic viscosity is a constant of proportionality. In computational fluid dynamics (CFD), governing equations for the blood flow in lumen domain are three-dimensional Navier–Stokes equations (which incorporate the density of the blood and dynamic viscosity) together with the continuity equation [16]. The solution, for a particular set of boundary conditions (e.g., prescribed inlet velocity profile which simulates cardiac cycle), provides the fluid velocity in a given geometry, which is in our case defined by geometric parameters.

TABLE I
Average Values of Input Parameters for AAA Model

Parameter	Mean value	Unit
Length	100	mm
Aneurysm length	40	mm
A	30	mm
Aorta diameter	20	mm
C	20	mm
B	20	mm
Density	0.00105	gr/mm^3
Dynamic viscosity	0.003675	Pa·s
Peak systolic velocity	300	mm/s

TABLE II
Average Values of Input Parameters for Carotid Bifurcation Model

Parameter	Mean value	Unit
Angle ICA-CCA	25	deg
Angle ECA-CCA	25	deg
Diameter of CCA	6.2	mm
Diameter of CBRE	3.658	mm
Diameter of CBRI	4.9	mm
Length of CCA	7.44	mm
Length of CBR	7.316	mm
Length of ECA	18.6	mm
Length of ICA	26.04	mm
Diameter at end of ICA	4.34	mm
Diameter of ICB	6.49	mm
Distance to ICB	5.39	mm
Density	0.00105	gr/mm^3
Dynamic viscosity	0.00367	Pa·s
Peak systolic velocity	437.22	mm/s

Sampling is performed from uniform distributions with perturbation of each parameter up to 30% of the corresponding mean values [16]. Tables I and II show the mean values of input variables used for sampling of AAA and carotid bifurcation model parameters, respectively.

The geometric parameters shown in Figs. 1 and 2 were used to generate internal blood vessel surfaces. Generated surfaces represent the boundaries for blood flow domain. We assumed that both AAA and carotid bifurcation have the same symmetry plane. Therefore, FE models were generated for half of the domain, but the results can be presented for the entire domain.

Unsteady simulations with parabolic inflow velocity profiles were undertaken and WSS distributions for each geometry were computed for 10 time steps ($N_t = 10$). We assumed the entering flow was pulsatile, with a typical waveforms shown in Fig. 3 for AAA [17] and carotid bifurcation [18] models. For each

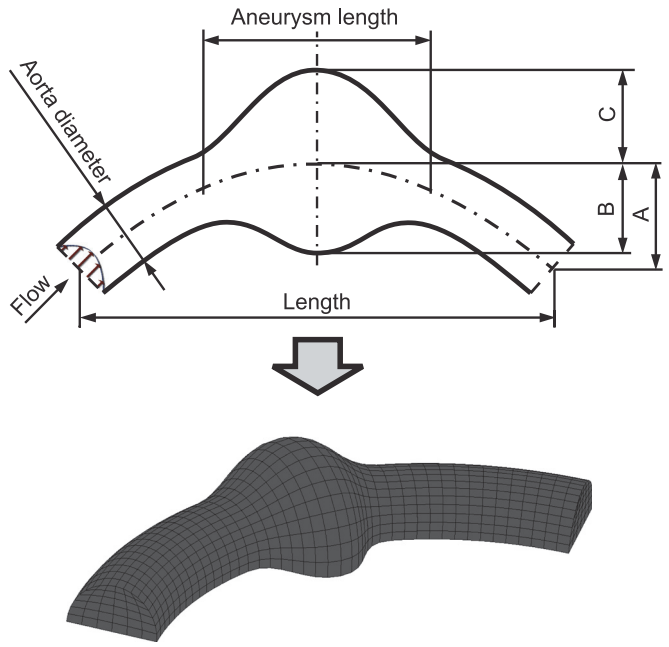

Fig. 1. Geometrically parameterized model of AAA. Geometrical parameters of AAA model: ′Length′ is the parameter that defines the total horizontal projection of the generated AAA model; ′A′ is the height of the arc of the central line; ′Aorta diameter′ is the abdominal aorta diameter; ′B′ is the radius from the central line to the inner wall of the aneurysm; ′C′ is the radius from the central line to the outer wall of the aneurysm; ′Aneurysm length′ is the average length of the aneurysm.

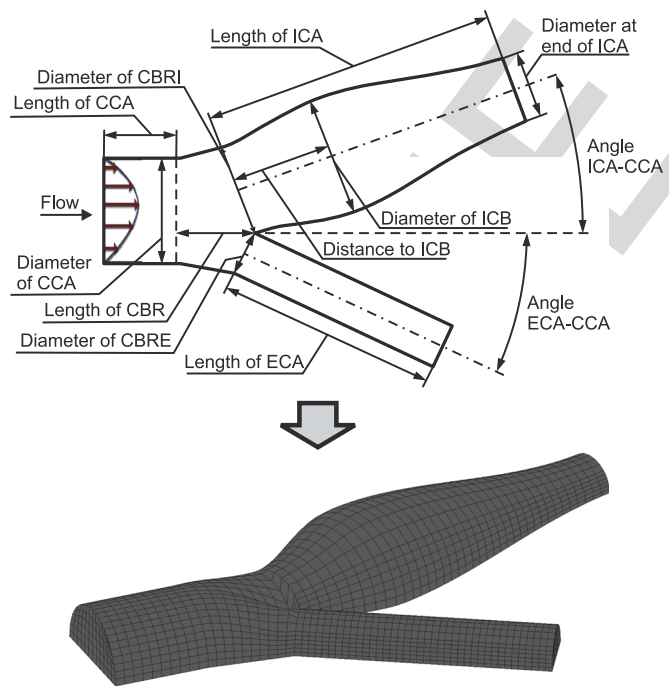

Fig. 2. Geometrically parameterized model of carotid bifurcation. The abbreviations here are: CCA−common carotid artery, CBR−carotid bifurcation region, CBRE−carotid bifurcation region external, ECA−external carotid artery, CBRI−carotid bifurcation region internal, ICA−internal carotid artery, ICB−internal carotid bulbus.

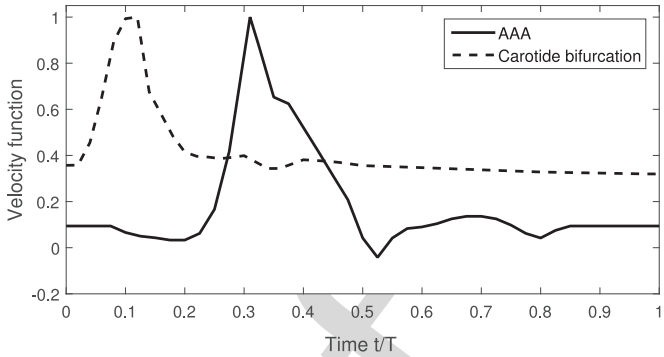

Fig. 3. Input velocity profile for the AAA [17] and carotid bifurcation [18] models. Inlet peak systolic velocity (PSV) corresponds to t/T = 0.305 and t/T = 0.1 for AAA and carotid bifurcation models respectively, where t/T is the relative time with respect to the cycle period T.

generated sample of both aneurysm and carotid bifurcation models, peak systolic velocity is sampled from the uniform distribution (bounded with 30% perturbation of the corresponding mean value) while velocity values in other time steps are calculated by multiplying the sampled peak systolic velocity value with the corresponding function given in Fig. 3. Mean values of the peak systolic velocity for aneurysm and carotid bifurcation models are adopted from [17] and [18], respectively.

All velocity components at the fixed walls are set to be zero. Similarly, the velocity components at the plane of symmetry in the direction normal to the plane, are set to zero. It is assumed that the end cross-sections of both AAA and carotid bifurcation models are stress-free, i.e., normal and tangential stresses are set to zero. The flow was assumed to be laminar, Newtonian, and incompressible. Also, the walls are assumed to be rigid. All calculations were performed using an open source FE program for fluid flow and fluid-solid interaction - PAK [15]. The CFD postprocessing results give an insight into the local hemodynamics and the blood mechanical action on the vessel walls, including the distribution of WSS.

In order to test whether the accuracy of the proposed machine learning based method for prediction of WSS distribution depends on the mesh resolution, we generated three datasets, each containing 4000 samples, with different mesh resolutions for both AAA and carotid bifurcation models. In these datasets, generated samples of the AAA FE model contain 375, 1125, and 2205 nodes, where 195, 597, and 885 lie on the wall surface, respectively. On the other hand, samples of the carotid bifurcation FE model contain 1854, 3877, and 5641 nodes, of which 642, 1303, and 1987 lie on the wall surface respectively. By using CFD simulations, WSS values were calculated in all surface nodes at the vessel wall for all datasets and for all samples for 10 time steps ($N_t = 10$; $t/T = \{0.1, 0.2, \ldots, 1\}$, where t/T is the relative time with respect to the cycle period T).

B. Unstructured Regression

Let us denote by $\mathbf{D} = \{\mathbf{x_i}, \mathbf{y_i}\}_{i=1,\ldots M}$ the dataset containing M observations, where $\mathbf{x_i} = (x_{i1}, \ldots, x_{iP})$ is one

observation with P features and $\mathbf{y_i} = (y_{i1}, \ldots, y_{iN})$ is a vector of real-valued output variables. The aim of multivariate (or multioutput) regression models is to learn a mapping $f : \mathbf{R}^P \rightarrow \mathbf{R}^N$ that predicts the vector of output variables $\mathbf{y_i}$ given an input vector $\mathbf{x_i}$.

1) Multivariate Linear Regression: The MLR model expresses an N-dimensional continuous response vector ($\mathbf{y_i}$) as a linear combination of predictor terms ($\mathbf{x_i}$) plus a vector of error terms ($\epsilon_\mathbf{i}$) with a multivariate normal distribution. In general, model may be written as

$$Y = XW + \epsilon \tag{1}$$

where $\mathbf{Y}$ is a MxN matrix with a series of multivariate measurements, $\mathbf{X}$ is a MxP design matrix, $\mathbf{W}$ is a PxN matrix containing parameters to be estimated, and ϵ is a matrix containing errors or noise. The errors are assumed to be uncorrelated across measurements.

2) MLP Neural Network: The MLP is a prediction model consisting of an input layer, one or more hidden layers and an output layer of simple elements called neurons. Neurons between different layers are connected with parameters called weights, which should be estimated through an optimization procedure (training). The objective of the training is to find a set of neural network parameters that minimize the error between the neural network predictions and the desired outputs. The most commonly used optimization algorithm for learning the parameters of neural network is the back-propagation algorithm [19]. However, the basic version of this algorithm has problems with slow convergence and local minima. For this purpose, a number of variations of the standard algorithm have been developed. In this study, we used the backpropagation algorithm with momentum and adaptive learning rate since it has been shown to be effective for the prediction of the WSS distribution [8], [9]. In each iteration of the this algorithm, parameters of the MLP are adjusted according to the following formula:

$$\Delta W_{\text{new}} = m_c \Delta W_{\text{prev}} + l_r m_c \frac{dE}{dW} \tag{2}$$

where W is a parameter vector, ΔW_{new} and ΔW_{prev} are the new and previous change of the parameter vector, respectively, m_c is a momentum constant, l_r is a learning rate, and E is the objective function which defines how much real outputs disagree with predicted ones (e.g., mean squared error). In each iteration (epoch) of the learning process, the learning rate is adjusted according to l_r^{inc}, l_r^{dec}, and $\max_{\text{inc}}$ parameters. Concretely, if performance decreases toward the goal, the learning rate is increased based on the l_r^{inc} parameter. On the other hand, if performance increases by more than the value defined by the $\max_{\text{inc}}$ parameter, the learning rate is adjusted based on the l_r^{dec} parameter.

In this study, we used an MLP neural network with ten neurons in a single hidden layer and sigmoid activation functions in hidden and output neurons. The stopping criterion was defined as the maximum number of learning epochs (1000). The values of other parameters were: $l_r = 0.01$, $m_c = 0.9$, $l_r^{\text{inc}} = 1.05$, $l_r^{\text{dec}} = 0.7$, and $\max_{\text{inc}} = 1.04$.

C. Structured Regression

A structured learning approach tries to simultaneously predict all outputs given all inputs and relationships among outputs. Structure learning methods can exploit correlation among output variables, which often gives benefits compared to unstructured learning methods. In other words, while traditional, unstructured models use only input information $\mathbf{x}$ to predict y_i, structured learning models use the additional information about y_j, for all j related to i. This prior information about interplays between the outputs $\mathbf{y}$ is application-specific and depends on prior beliefs of a practitioner about which relationships might be useful.

Conditional random fields (CRF) is a type of discriminative probabilistic graphical model designed to predict structured output. Originally, CRF were proposed for classification of sequential data [20].

The conditional distribution $P(\mathbf{y}|\mathbf{x})$ for CRF can be represented as

$$P(\mathbf{y}|\mathbf{x}) = \frac{1}{Z(\alpha, \beta, \mathbf{x})} e^{\sum_{i=1}^{N} A(\alpha, y_i, \mathbf{x}) + \sum_{i \sim j} I(\beta, y_i, y_j, \mathbf{x})} \tag{3}$$

where $A(\alpha, y_i, \mathbf{x})$ is an association potential with parameters α, $I(\beta, y_i, y_j, \mathbf{x})$ is an interaction potential with parameters β, $i \sim j$ denotes that y_i and y_j are connected by an edge in the graph structure, and $Z(\alpha, \beta, \mathbf{x})$ represents a normalization function. In general, the output y_i is associated with a vector of observation $\mathbf{x}$ by an association function, while relationships among outputs can be modeled by an interaction function. Association and interaction potential are usually defined as linear combinations of a set of feature functions over *K*-dimensional parameters α and *L*-dimensional parameters β [20]:

$$A(\alpha, y_i, \mathbf{x}) = \sum_{k=1}^{K} \alpha_k f_k(y_i, \mathbf{x}) \tag{4}$$

$$I(\beta, y_i, y_j, \mathbf{x}) = \sum_{l=1}^{L} \beta_l g_l(y_i, y_j, \mathbf{x}). \tag{5}$$

Feature functions are convenient since they allow one to model arbitrary interplays between inputs and outputs. In this way, any potentially relevant feature may be included to the model since their relevance is automatically determined through the parameter estimation process.

The learning task is to determine values of parameters α and β to maximize the conditional log-likelihood of the set of training examples:

$$L(\alpha, \beta) = \log P(\mathbf{y}|\mathbf{x}) \tag{6}$$

$$(\hat{\alpha}, \hat{\beta}) = \text{argmax}_{\alpha,\beta}(L(\alpha, \beta)). \tag{7}$$

On the other hand, given estimated parameters $\hat{\alpha}$ and $\hat{\beta}$ and inputs $\mathbf{x}$, the inference task is to find the point estimate $\hat{\mathbf{y}}$ of outputs $\mathbf{y}$ such that the conditional probability $P(\mathbf{y}|\mathbf{x})$ is maximized:

$$\hat{\mathbf{y}} = \text{argmax}_{\mathbf{y}}(P(\mathbf{y}|\mathbf{x})). \tag{8}$$

Models with real valued outputs pose quite different challenges with respect to feature function complexity compared to discrete-valued case. CRFs were originally designed for classification problems where the normalizing function Z is finite and defined as a sum over finitely many possible values of $\mathbf{y}$. On the contrary, for regression, Z must be an integrable function. In general, providing that Z is integrable can be very difficult and computationally expensive due to the complexity of association and interaction potentials. However, the association and interaction potentials could be designed in a way that allows efficient learning and inference.

The selection of appropriate feature functions in CRF is a manual process which is usually application-specific. However, the choice of features is often constrained to simple constructs to reduce the complexity of learning and inference from CRF. Let us assume we are given K *unstructured (baseline) predictors*, $R_k(\mathbf{x})$, k = 1, ...K, that predict single output y_i relying on any subset of $\mathbf{x}$. To model the dependency between the prediction and output, we use quadratic feature functions:

$$f_k(y_i, \mathbf{x}) = -(y_i - R_k(\mathbf{x}))^2. \tag{9}$$

These feature functions follow the basic principle for association potentials, i.e., their values are large when predictions and outputs are similar. To model the correlation among outputs, we use the quadratic feature function:

$$g_l(y_i, y_j, \mathbf{x}) = -e^l_{\mathrm{ij}} S^l_{\mathrm{ij}}(\mathbf{x})(y_i - y_j)^2 \tag{10}$$

where $e_{ij} = 1$ if an edge exists between output y_i and y_j in the graph G_l, and $e_{ij} = 0$ otherwise; $S^l_{ij}(\mathbf{x})$ represents the similarity between outputs y_i and y_j and in general depends on inputs $\mathbf{x}$. The larger the value of $S^l_{ij}(\mathbf{x})$ is, the more similar the outputs y_i and y_j are. It should be noted that using multiple graphs G_l can facilitate modeling of different aspects of correlation between outputs.

In this way, the exponent of the probability distribution $P(\mathbf{y}|\mathbf{x})$ is a quadratic function in terms of $\mathbf{y}$. Therefore $P(\mathbf{y}|\mathbf{x})$ can be transformed into the multivariate Gaussian distribution $\mathcal{N}(\mu(\mathbf{x}), \mathbf{\Sigma}(\mathbf{x}))$:

$$P(\mathbf{y}|\mathbf{x}) = \frac{1}{(2\pi)^{N/2}\,|\mathbf{\Sigma}|^{1/2}} \times \exp\left(-\frac{1}{2}(\mathbf{y}-\mu)^T \mathbf{\Sigma}^{-1}(\mathbf{y}-\mu)\right) \tag{11}$$

where $\mathbf{\Sigma}$ and μ are covariance matrix and mean vector, respectively. Therefore, the resulting conditional distribution is Gaussian with mean μ and covariance $\mathbf{\Sigma}$. We observe that $\mathbf{\Sigma}$ is a function of parameters α and β, and interaction potential graphs G_l, while μ is also a function of inputs $\mathbf{x}$. The resulting CRF is the Gaussian CRF.

Since the model is Gaussian, the inference is straightforward, i.e., the prediction is expected value, which is equal to the mean μ of the distribution:

$$\hat{\mathbf{y}} = \mathrm{argmax}_{\mathbf{y}} P(\mathbf{y}|\mathbf{x}) = \mathbf{\Sigma}\mathbf{b}. \tag{12}$$

III. Results

A. Evaluation Procedure

In this paper, we employed two unstructured models, MLP neural network and the MLR model, as well as GCRF, in order to predict WSS distributions through time. For training the GCRF model, we randomly chose 70% of total data and remaining 30% of data was used for testing. Since we use predictions of both unstructured models MLP and MLR as inputs to GCRF, we applied fivefold cross validation on the training set. First, for both AAA and carotid bifurcation, we split the training set into five subsets ($D_i, i = 1, \ldots, 5$) of equal sizes. Then, we reserved one dataset D_i for testing and merged data from the remaining four datasets $D_j, j \neq i$ for training. The procedure was repeated five times, for $i = 1, \ldots, 5$. Finally, we got MLP and MLR predictions for all samples in training sets.

For each surface node, we constructed one MLR model with N_t outputs, where each of N_t outputs represent WSS value for a single time step (N_t is the number of time steps). This means that we created 195, 597, and 885 (642, 1303, and 1987) different linear models in case of the AAA (carotid bifurcation) model. The features of the MLR model were geometric parameters of models, blood density, dynamic viscosity and velocities in all time steps. More specifically, we used 18 features in of the AAA model and 24 features in case of the carotid bifurcation model. The same procedure is repeated for the MLP model where we create one neural network for each node.

In order to employ the GCRF model to predict WSS distribution, we define the similarity matrix (graph) between different surface nodes. Let $S_i = (x_i, y_i, z_i)$ and $S_j = (x_j, y_j, z_j)$ be coordinates of the ith and jth surface nodes, respectively. The distance between two nodes is calculated as the Euclidean distance:

$$d(S_i, S_j) = \sqrt{(x_i - x_j)^2 + (y_i - y_j)^2 + (z_i - z_j)^2}. \tag{13}$$

In order to eliminate noise in the similarity matrix, we eliminated similarities of some nodes that are far away from each other. We calculate similarity matrix between the ith and jth node as

$$S(i,j) = \begin{cases} 0, & \text{if } d(S_i, S_j) > \mu_d \\ 1 - \dfrac{d(S_i, S_j) - \min_d}{\mu_d - \min_d}, & \text{otherwise} \end{cases} \tag{14}$$

where $\min_d$, and μ_d are minimum and mean values of all distances between nodes, respectively.

For each training example and for each time step, we trained a different GCRF model. In this way, we estimated different parameters α and β for each training example. Our proposed model predicts the target values for a test example in the following way. First, it finds the most similar training example (the nearest neighbor) and then uses its estimated parameters α and β to predict the evolution of WSS distributions through time.

We evaluated the performances of the proposed models by computing their coefficients of determination R^2. In a general form, R^2 can be seen as the fraction of unexplained variance. In order to define the coefficient of determination at tth time step

TABLE III
PERFORMANCES FOR AAA MODEL

Dataset (nodes)	Model	t_1	t_2	t_3	t_4	t_5	t_6	t_7	t_8	t_9	t_{10}	Average
AAA (375)	MLR	0.964	0.963	0.957	0.936	0.857	0.765	0.850	0.745	0.827	0.837	0.870
	MLP	0.948	0.982	0.982	0.971	0.934	**0.898**	0.931	**0.883**	0.887	0.806	0.922
	GCRF	**0.969**	**0.984**	**0.984**	**0.972**	**0.935**	**0.898**	**0.932**	**0.883**	**0.894**	**0.853**	**0.930**
AAA (1125)	MLR	0.957	0.960	0.957	0.939	0.939	0.774	0.868	0.734	0.849	0.855	0.883
	MLP	**0.988**	**0.987**	0.990	0.985	0.985	0.862	0.953	0.766	0.917	0.865	0.930
	GCRF	0.986	**0.987**	**0.991**	**0.987**	**0.987**	**0.875**	**0.955**	**0.814**	**0.922**	**0.894**	**0.940**
AAA (2205)	MLR	0.955	0.956	0.953	0.933	0.851	0.774	0.861	0.739	0.842	0.839	0.870
	MLP	0.961	0.982	0.986	0.976	0.940	**0.929**	0.965	0.883	0.944	0.858	0.942
	GCRF	**0.974**	**0.983**	**0.988**	**0.978**	**0.942**	**0.929**	**0.966**	**0.885**	**0.945**	**0.886**	**0.948**

TABLE IV
PERFORMANCES FOR CAROTID BIFURCATION MODEL

Dataset (nodes)	Model	t_1	t_2	t_3	t_4	t_5	t_6	t_7	t_8	t_9	t_{10}	Average
Carotid (1854)	MLR	0.767	0.740	0.761	0.762	0.762	0.763	0.762	0.763	0.763	0.764	0.761
	MLP	0.873	0.930	**0.963**	**0.968**	**0.980**	**0.978**	0.957	0.946	0.932	0.879	0.941
	GCRF	**0.904**	**0.934**	0.960	**0.968**	**0.980**	**0.978**	**0.959**	**0.950**	**0.937**	**0.909**	**0.948**
Carotid (3877)	MLR	0.803	0.768	0.768	0.768	0.793	0.794	0.794	0.794	0.795	0.795	0.787
	MLP	0.850	0.891	**0.966**	**0.985**	**0.985**	**0.985**	**0.982**	**0.964**	0.911	0.880	0.940
	GCRF	**0.908**	**0.914**	**0.966**	**0.985**	**0.985**	**0.985**	0.979	**0.964**	**0.933**	**0.917**	**0.954**
Carotid (5641)	MLR	0.791	0.762	0.781	0.782	0.782	0.782	0.782	0.782	0.783	0.783	0.781
	MLP	0.845	**0.910**	0.960	**0.980**	**0.983**	**0.974**	**0.974**	**0.959**	**0.945**	0.831	0.936
	GCRF	**0.895**	**0.910**	**0.961**	0.973	**0.983**	**0.974**	**0.974**	**0.959**	**0.945**	**0.891**	**0.946**

R_t^2, let us define $\overline{y}^t(j)$ as the mean value of WSS for the jth surface node at time step t:

$$\overline{y}^t(j) = \frac{1}{N_{\text{test}}} \sum_{i=1}^{N_{\text{test}}} y_i^t(j),$$
$$t = 1, \dots N_t, j = 1, \dots, N_{\text{surf}} \tag{15}$$

where N_{test} is the number of testing examples, N_{surf} is the number of surface nodes, and $y_i^t(j)$ is the WSS value for jth node at tth time step of ith example calculated by the finite element method (FEM). The sum of squares (proportional to the variances) $\overline{SE}_i^t$ for the ith example at time step t is calculated as

$$\overline{SE}_i^t = \sum_{j=1}^{N_{\text{surf}}} (y_i^t(j) - \overline{y}^t(j))^2. \tag{16}$$

The residuals are defined as a squared error of the ith example at time step t:

$$SE_i^t = \sum_{j=1}^{N_{\text{surf}}} (y_i^t(j) - \hat{y}_i^t(j))^2 \tag{17}$$

where $\hat{y}_i^t(j)$ is the predicted WSS value for jth surface node at tth time step of ith example. Finally, the coefficient of determination R_t^2 at tth time step is calculated as

$$R_t^2 = 1 - \frac{\sum_{i=1}^{N_{\text{test}}} SE_i^t}{\sum_{i=1}^{N_{\text{test}}} \overline{SE}_i^t}. \tag{18}$$

B. Performance on AAA and Carotid Bifurcation

In order to make a fair comparison, we trained unstructured models (MLP neural network and MLR) on the same data used for GCRF training. Tables III and IV show obtained results on the same test data for AAA and carotid bifurcation models, respectively. Values in these tables represent coefficient of determination R_t^2, for each time step $t = 1, \dots, 10$, along with the average R^2 across all time steps.

Tables III and IV clearly show that the MLP model outperforms the MLR model on both AAA and carotid bifurcation models. More precisely, on the AAA(375) dataset, the MLP achieved higher accuracy compared to the MLR in eight out of ten time steps. In addition, on the AAA(1125) and AAA(2205) datasets, the MLP outperformed the MLR in all time steps. Similar results are obtained on carotid bifurcation datasets where the MLP achieved higher accuracy compared to the MLR in all time steps for all three mesh resolutions (1854, 3877, and 5641 nodes). The fact that the MLP improved accuracy over the MLR model is confirmed by the average R^2 values across all time steps (the last columns in Tables III and IV). Even though the MLP outperforms the MLR on all datasets, results given in Tables III and IV indicate that both the MLP (better) and the MLR (worse) can be used to predict WSS distribution through time. This confirms the first hypothesis of our paper that WSS distributions at different cardiac cycle time points for geometrically parameterized models of AAA and carotid bifurcation can be modeled by using machine learning approaches.

In addition, Tables III and IV show that the GCRF model achieved higher accuracy compared to unstructured predictors

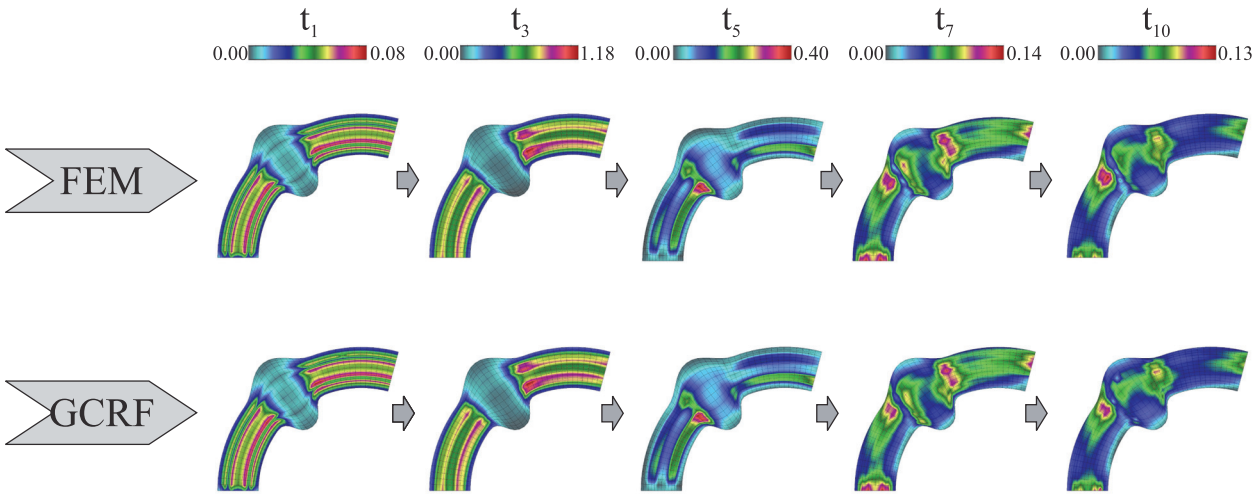

Fig. 4. Temporal evolution of WSS distribution for the AAA model (one randomly chosen geometry) calculated by FEM and predicted by the GCRF (units Pa). Due to space limitation we show results for only five time steps (of total ten).

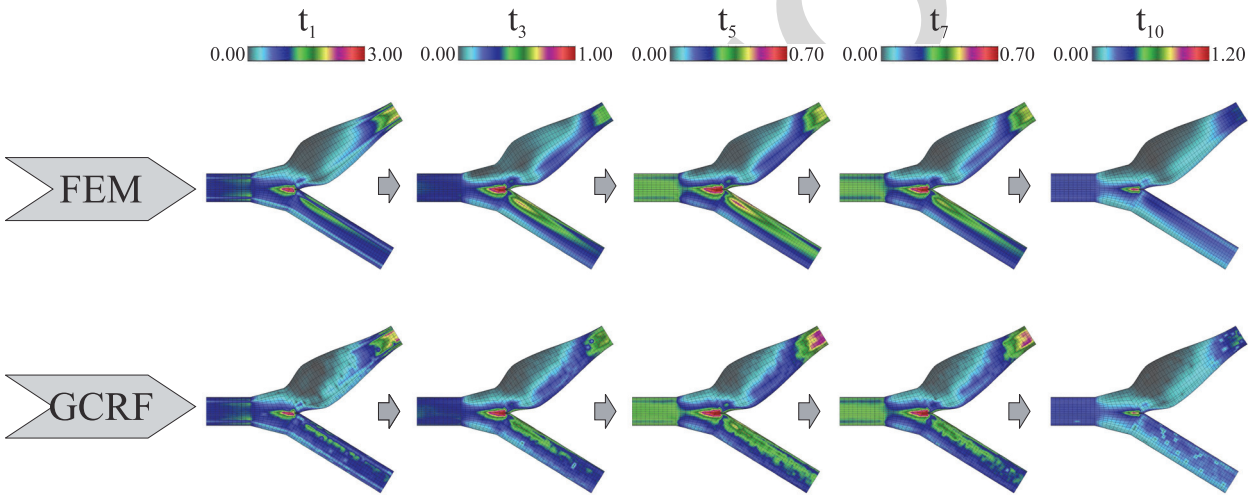

Fig. 5. Temporal evolution of WSS distribution for the carotid bifurcation model (one randomly chosen geometry) calculated by FEM and predicted by the GCRF (units Pa). Due to space limitation we show results for only five time steps (of total ten).

(MLP and MLR) on both datasets. More precisely, on the AAA(375) dataset, the GCRF outperformed the MLP model in eight out of ten time steps, while on the remaining two steps they achieved the same accuracy. Furthermore, on AAA(1124) dataset, the GCRF achieved higher accuracy compared to the MLP model in eight out of ten time steps, while on one step they achieved the same accuracy. Similarly, on the AAA(2205) dataset, the GCRF achieved higher accuracy compared to the MLP model in nine out of ten time steps, while on the remaining step they achieved the same accuracy. Similar results can be observed on the carotid bifurcation dataset. More specifically, on Carotid(1854) dataset, the GCRF outperformed the MLP model in six out of ten time steps, while they achieved the same accuracy in three steps. Similarly, on the Carotid(3877) dataset, the GCRF achieved higher accuracy compared to the MLP model in four out of ten time steps, while they achieved the same accuracy in five time steps. On the Carotid(5641) dataset, GCRF outperformed the MLP model in three out of ten time steps, while they achieved the same accuracy six steps. In addition, GCRF outperformed MLR in all time steps for all AAA and carotid bifurcation datasets. The average values of R^2 calculated across all time steps show that the GCRF model outperformed both unstructured predictors. These results confirm the second hypothesis of our paper, i.e., taking spatial correlation into account improves prediction accuracy of WSS distribution through time.

Figs. 4 and 5 show the distribution of WSS through time, calculated by FEM and predicted by the GCRF model. Due to lack of space, we showed results only for one randomly chosen test example from AAA and carotid bifurcation datasets in five time steps (t_1, t_3, t_5, t_7, and t_{10}). These figures confirm the ability of machine learning approaches to predict the WSS distribution through time for both geometrically parameterized models.

In addition, we compared running time of FEM and GCRF methods for prediction of WSS distribution of AAA and carotid

bifurcation models. Training of the GCRF model for prediction of WSS distribution is a tedious task. However, once trained this model can be utilized to predict WSS distribution in much shorter time when comparing to FEM approach. For instance, average FEM run time for calculation of WSS distribution of testing samples was 5.3, 6.8, and 8.0 s for the three datasets of the AAA model and 19.4, 198.4, and 604.1 for the three datasets of the carotid bifurcation model. On the other hand, the corresponding average GCRF run times were 0.032, 0.283, and 0.604 s for the AAA model and 0.5702, 5.856, and 10.937 for the carotid bifurcation model. All the experiments were run on a Windows machine with a 3.40 GHz Intel(R) Core(TM) i7-3770 CPU and 32GB memory.

IV. Conclusion

In this paper, an application of machine learning techniques to hemodynamic problems was presented. We modeled the relationships between geometric parameters, blood density, dynamic viscosity and velocity of the human carotid bifurcation, and AAA models and the WSS distribution. The goal of this paper is to verify that for geometrically parameterized models, which are simplified comparing to real geometries, machine learning approaches may be used to predict WSS distribution at different cardiac cycle time points. We employed two unstructured predictors, MLP neural network and the MLR model, in order to predict WSS distributions through time. The obtained results showed that on the AAA model both predictors exhibited capabilities of being used for this task, while on the carotid bifurcation model MLP demonstrated much better results in terms of R^2. In addition, we applied the GCRF model, which leverages the benefits of both unstructured models as well as the similarities between different surface nodes. The results obtained from simulations showed that GCRF was able to improve accuracy on both AAA and carotid bifurcation models. Furthermore, this work shows that the achieved results can be used to aid the assessment of stroke risk for a given patient's data in real time.

Further research will be focused on applying other unstructured multioutput regression models and including them into the GCRF model. In addition, since we used simplified geometrically parameterized models, our further research plan is to use real life data, where machine learning techniques will be tested on patient data. More specifically, we plan to represent a real arterial geometry with an adequate geometrically parameterized model and predict WSS distribution for the simplified model. Thereafter, WSS value of each surface node of the real arterial geometry can be estimated by interpolating WSS values of the nearest nodes of the simplified model. However, real arterial geometries are quite complex and describing them with a set of features that can be further processed by machine learning methods to predict WSS distribution is a challenging task. Therefore, we plan to extend the proposed approach where, in addition to geometrical parameters which can be estimated from medical images, machine learning approaches would also use other node specific descriptors (e.g., coordinates, distance from the central line, local curvature descriptors, cross section area, etc.) to predict the WSS value. In this case, instead of node specific predictors, we would generate a global predictor which would predict WSS values for all nodes belonging to a certain arterial region (for instance all nodes in the internal carotid bulbus region).

References

[1] U. G. Schulz and P. M. Rothwell, "Sex differences in carotid bifurcation anatomy and the distribution of atherosclerotic plaque," *Stroke*, vol. 32, no. 47, pp. 1525–1531, Jul. 2001.

[2] U. G. Schulz and P. M. Rothwell, "Major variation in carotid bifurcation anatomy: a possible risk factor for plaque development," *Stroke*, vol. 32, no. 11, pp. 2522–2529, Nov. 2001.

[3] S. Lorthois, P. Lagree, J. Marc-Vergnes, and F. Cassot, "Maximal wall shear stress in arterial stenoses: Application to the internal carotid arteries," *ASME J. Biomech. Eng.*, vol. 12, pp. 661–666, 2000.

[4] L. Boussel *et al.*, "Aneurysm growth occurs at region of low wall shear stress: Patientspecific correlation of hemodynamics and growth in a longitudinal study," *Stroke*, vol. 38, no. 11, pp. 2997–3002, 2008.

[5] J. Xiang *et al.*, "Hemodynamic-morphologic discriminants for intracranial aneurysm rupture," *Stroke*, vol. 42, no. 1, pp. 144–152, 2011.

[6] A. Malek, S. Alper, and S. Izumo, "Hemodynamic shear stress and its role in atherosclerosis," *J. Amer. Med. Assoc.*, vol. 282, no. 21, pp. 2035–2042, 1999.

[7] M. Akram and J. Andre, "Wall shear stress and early atherosclerosis," *Amer. J. Roentgenology*, vol. 174, no. 6, pp. 1657–1665, 2000.

[8] M. Radovic, D. Petrovic, and N. Filipovic, "Mining data from cfd simulation for aneurysm and carotid bifurcation models," in *Proc. 33rd Annu. Int. Conf. IEEE Eng. Med. Biol. Soc.*, Sep. 2011, pp. 8311–8314.

[9] Z. Bosnic, P. Vracar, M. Radovic, G. Devedzic, N. Filipovic, and I. Kononenko, "Mining data from hemodynamic simulations for generating prediction and explanation models," *IEEE Trans. Inf. Technol. Biomed.*, vol. 16, no. 2, pp. 248–254, Mar. 2012.

[10] V. Radosavljevic, S. Vucetic, and Z. Obradovic, "Continuous conditional random fields for regression in remote sensing," in *Proc. 2010 19th Eur. Conf. Artif. Intell.*, 2010, pp. 809–814.

[11] J. Glass, M. Ghalwash, M. Vukicevic, and Z. Obradovic, "Extending the modeling capacity of gaussian conditional random fields while learning faster," in *Proc. 30th AAAI Conf. Artif. Intell.*, Feb. 2016, pp. 1–4.

[12] J. Slivka, M. Nikolic, K. Ristovski, V. Radosavljevic, and Z. Obradovic, "Distributed gaussian conditional random fields based regression for large evolving graphs," in *Proc. 14th SIAM Int. Conf. Data Mining, Workshop Mining Netw. Graphs*, Apr. 2014. Q2

[13] N. Djuric, V. Radosavljevic, Z. Obradovic, and S. Vucetic, "Gaussian conditional random fields for aggregation of operational aerosol retrievals," *IEEE Geosci. Remote Sens. Lett.*, vol. 12, no. 4, pp. 761–765, Apr. 2015.

[14] A. Polychronopoulou and Z. Obradovic, "Hospital pricing estimation by gaussian conditional random fields based regression on graphs," in *Proc. 2014 IEEE Int. Conf. Bioinformat. Biomed.*, Nov. 2014, pp. 564–567.

[15] M. Kojic, N. Filipovic, R. Slavkovic, M. Zivkovic, and N. Grujovic, "Pak-fs - Finite element program for fluid flow and fluid-solid interaction," University of Kragujevac and R&D Center for Bioengineering, Kragujevac, Serbia, 1998.

[16] M. Kojic, N. Filipovic, B. Stojanovic, and N. Kojic, *Computer Modeling in Bioengineering: Theoretical Background, Examples and Software*. Hoboken, NJ, USA: Wiley, 2008.

[17] C. M. Scotti, A. D. Shkolnik, S. C. Muluk, and E. A. Finol, "Fluid-structure interaction in abdominal aortic aneurysms: effects of asymmetry and wall thickness," *Biomed. Eng. Online*, vol. 4, 2005, Art. no. 64.

[18] K. Perktold, M. Resch, and R. O. Peter, "Three-dimensional numerical analysis of pulsatile flow and wall shear stress in the carotid artery bifurcation," *J. Biomech.*, vol. 24, no. 6, pp. 409–420, 1991.

[19] D. E. Rumelhart, G. E. Hinton, and R. J. Williams, *Parallel Distributed Processing: Explorations in the Microstructure of Cognition*, vol. 1, D. E. Rumelhart, J. L. McClelland, and C. PDP Research Group, Eds. Cambridge, MA, USA: MIT Press, 1986.

[20] J. D. Lafferty, A. McCallum, and F. C. N. Pereira, "Conditional random fields: Probabilistic models for segmenting and labeling sequence data," in *Proc. 18th Int. Conf. Mach. Learn.*, 2001, pp. 282–289.

Authors' photographs and biographies not available at the time of publication.

Queries

Q1. Authors: When accessing and uploading your corrections at the Author Gateway, please note we cannot accept new source files as corrections for your paper. Please do not send new Latex, Word, or PDF files, as we cannot simply "overwrite" your paper. Please submit your corrections as an annotated PDF or as clearly written list of corrections, with location in paper. You can also upload revised graphics to the Gateway.

Q2. Author: Please provide page range in Ref. [12].